Electronic Supplementary Information (ESI)

Controlling Microgel Deformation via Deposition Method and Surface Functionalization of Solid Supports

Laura Hoppe Alvarez, Andrey A. Rudov, Rustam A. Gumerov, Pia Lenssen, Ulrich Simon, Igor I. Potemkin and Dominik Wöll

1. Supporting 3D representations of the super-resolved microgels

The 3D points clouds resulting for the super-resolved imaging of the 3 x 3 different systems presented in Fig. 3 of the main paper are provided as movies in the ESI:

- 01_PEG_adsorption_z_rotation.mp4
- 02_GLASS_adsorption_z_rotation.mp4
- 03_FOCTS_adsorption_z_rotation.mp4
- 04_PEG_dropcasting_z_rotation.mp4
- 05_GLASS_dropcasting_z_rotation.mp4
- 06_FOCTS_dropcasting_z_rotation.mp4
- 07_PEG_spincoating_z_rotation.mp4
- 08_GLASS_spincoating_z_rotation.mp4
- 09_FOCTS_spincoating_z_rotation.mp4

2. Model for Simulations

The LAMMPS package[S1] was used to perform molecular dynamics (MD) simulations within a standard coarse-grained model with explicit solvent. The simulations were carried out in the NVT ensemble in reduced (dimensionless) units derived from the potential parameters, ε and σ, the mass m of a single particle and Boltzmann's constant, k_B. The equations were integrated with a time step, $\Delta t = 0.005\,\tau$, where $\tau = \sigma\,(m/\varepsilon)^{0.5}$ is the standard time unit for a Lennard-Jones (LJ) fluid. We set the temperature in the system, $T = 0.72\,\varepsilon/k_B$, and maintain it using the Nose-Hoover thermostat. The temperature is chosen in range between the triple-point temperature[S2] $T = 0.65\,\varepsilon/k_B$, and the critical temperature[S3] $T = 1.08\,\varepsilon/k_B$, of the LJ fluid such a way to represent the vapor/liquid coexistence.

All systems contain two different types of particles: liquid/vapor water beads, W, and microgel beads, M (Table S1). The W and M beads have the same diameter σ, the same mass m, and are defined by the truncated force-shifted Lennard-Jones potential:

$$U_{LJ\,smo}(r) = \varphi_{LJ}(r) - \varphi_{LJ}(r_{cut}) - (r - r_{cut})\frac{d\varphi_{LJ}}{dx} \quad (1)$$

$$\varphi_{LJ}(r) = \begin{cases} 4\varepsilon_{ij}\left(\left(\frac{\sigma}{r}\right)^{12} - \left(\frac{\sigma}{r}\right)^{6}\right), & r \le r_{cut} \\ 0, & r > r_{cut} \end{cases} \quad (2)$$

where $r_{cut} = 2.5\,\sigma$, $i, j \in \{W, M\}$.

The efficient application of the LJ potential in molecular simulations of a bulk and the interfacial properties of simple fluids with appropriate values for the size and energy parameters σ and ε are well described.[S4–S8] We set the parameter of interaction between water-water beads $\varepsilon_{WW} = 1\,\varepsilon$ (see also Fig. S1).

Table S1: MD interaction parameters (in units of ε) at $T = 0{,}72\varepsilon/k_B$ used in simulations, where ε refers to the LJ energy parameter of the fluid−fluid interaction and k_B is the Boltzmann constant.

	M	**W**	**S**	**T**
M	0.275	1	ε_{MS}	0.001
W		1	ε_{WS}	0.001
S			–	–
T				–

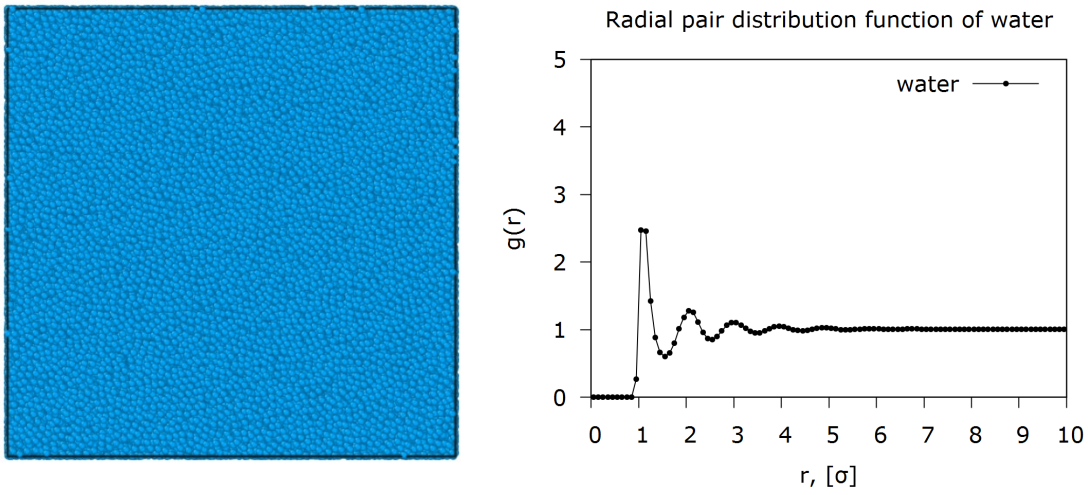

Figure S1: (Left) Schematic illustration of the simulation box fulfilled by water beads. (Right) Radial pair distributions function of liquid at $T = 0{,}72\varepsilon/k_B$. Liquid density $\rho = 0.8/\sigma^3$.

The µG was designed as described previously.[S9, S10] It consists of fully stretched chains of equal length, *n* = 15 beads, which are connected through tetrafunctional cross-linker beads. The fraction of the cross-linkers for such microgels is around 0.03 which correlates to the amount of crosslinker used in the synthesis. The total number of beads of type M in the final structure was 8000. The connectivity of the beads into a polymer network was maintained by the combination of the finite extension nonlinear elastic (FENE) potential and Lennard-Jones potential:

$$U_{bond}(r) = U_{FENE}(r) + U_{LJ}(r) \tag{3}$$

where the distance between two beads is denoted by r.

$$U_{FENE}(r) = -\frac{1}{2}KR_{max}{}^2\ln(1-\frac{r^2}{R_{max}{}^2}) \quad (4)$$

$$U_{LJ}(r) = 4\varepsilon_{bond}\left[\left(\frac{\sigma}{r}\right)^{12} - \left(\frac{\sigma}{r}\right)^{6}\right] + \varepsilon_{bond} \quad (5)$$

with the spring constant, $K = 20.6\,\varepsilon/\sigma^2$, the maximum bond length, $R_{max} = 1.5\,\sigma$, $\varepsilon_{bond} = 1\,\varepsilon$, and the cutoff radius $r_{cut} = 2^{1/6}\,\sigma$.

We have identified characteristic interaction parameters that correspond to good, θ and bad solvent. To mimic the swollen state of the microgel in the bulk solution, we set the value of the LJ parameter for the microgel bead-to-bead-interactions to $\varepsilon_{MM} = 0.275\,\varepsilon$ and for the microgel-water-interaction to $\varepsilon_{MW} = 1\,\varepsilon$. The idea behind these is as follows: at $\varepsilon_{MW} = 1\,\varepsilon$, all subchains of the microgel in the bulk are elongated, providing reasonable swelling of the microgel (see Fig. S2). At the same time in the absence of solvent (after the complete evaporation of the liquid) the microgel should be in the collapsed state. At the given temperature the microgel is appeared to be in a collapsed state if $\varepsilon_{MM} \geq 0.227\varepsilon$. The higher the ε_{MM} the more chances to observe the "frozen" behavior of the microgel at the same collapsed state. Moreover, spreading of the microgel on the surface at high ε_{MM} will require high ε_{MS} value which will lead to unphysical results.

The study of adsorption of the microgel from the bulk to the substrate was performed in a simulation box with the dimensions $L_x = L_y = 110\,\sigma$, $L_z = 80\,\sigma$ while the investigation of the microgels in the drying droplet at the substrate was done in a simulation box with the dimensions $L_x = L_y = 230\,\sigma$; $L_z = 100\,\sigma$.

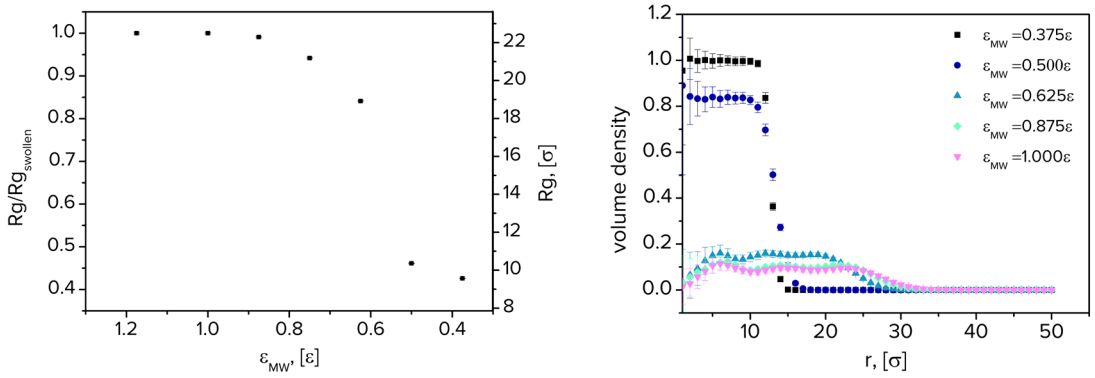

Figure S2: (Left) Swelling degree of the microgel depending on the microgel/water interaction parameter, ε_{MW}. (Right) Volume fraction of beads of the microgel as a function of a distance from the center of mass of the microgel for different interaction parameter ε_{MW}.

We introduced two smooth solid flat walls on opposite sides of the simulation box: S at $z = 0$ and U at $z = L_z$, represented by a LJ potential (Eq. 2). Thus, we obtain a 2D+1 slab geometry, and periodic boundary conditions are applied only in *x*, *y* directions. The force acts on each bead in the system in ***z*** direction perpendicular to the wall if the distance between them and the wall is less than $r_{cut\,wall} = 3\sigma$. The bottom wall performs the role of the substrate. Such "simplification" of the substrate description is quite reasonable, keeping in mind that the roughness of the glass surface as well as the thickness of FOCTS and PEG coating is much smaller than the size of the microgel.[S9] In general, the intrinsic contact angle θ depends on roughness and the density of the substrate,[S11, S12] ρ_s, the LJ energy parameter of the substrate−droplet interaction and the temperature T of the system.[S13] In our case with sufficient accuracy (due to the fact that the modification was done with high surface coverage value, f = 0.91 for FOCTS and f ~1 for PEG[S9]) we focused only on the effect of hydrophobicity/hydrophilicity of the surface at a given temperature. Varying the water-substrate, ε_{WS}, and microgel-interaction parameter, ε_{MS}, we could control the affinity of the substrate for the liquid and polymer beads, and as a result, change the contact angle of the droplet θ. We set all interaction parameters between the upper wall and every beads in the system as $\varepsilon_{iU} = 0{,}001\,\varepsilon$, $i \in \{W, M\}$ which corresponds to complete repulsion.

We consider two types of systems. The first one is a drying droplet at the substrate. The initial configuration is as follows: the liquid phase with a presence of the single swollen microgel floating in the vicinity of the droplet is placed in the form of a sphere of radius *R* = 80 and a contact angle of ~ 180° on the wall (see Fig. 4 in the main paper). The sphere is surrounded by a vapor phase. The density of both fluid phases is chosen according to their values at saturation for given dimensions of the system. ε_{WS} is chosen as $1.7\ \varepsilon$, $2.75\ \varepsilon$, or $3.25\ \varepsilon$ to obtain the intrinsic contact angles of the pure liquid of $\theta \sim 100°$, $\sim 54°$ and $27°$ for FOCTS, glass and PEG substrate, respectively (see Fig. 1 in the main paper). After 10^7 timesteps of the equilibration run, we started to investigate the evaporation of the solvent from the droplet. In drop-casting experiment the temperature of the substrate as well as the ambient temperature is kept constant. The difference in the vapor pressure close to a droplet surface and the ambient (partial) pressure of the vapor far away from the drop drives a diffusive flux, leading to droplet evaporation. Among different techniques in MD allowing to simulate the droplet evaporation process, we used the following method. We remove water vapor beads from the system to shift the balance between condensation and evaporation. The rate of droplet evaporation is controlled by the number of removed particles and the removal frequency. Virtual sphere having the radius $R = 90\ \sigma$ and center coincided with the center of mass of the droplet was introduced in the system. It is important that the droplet is entirely situated within that region every single time step. To study the effect of the evaporation rate on the deposit pattern, we removed vapor molecules at different rates from the simulation; namely, one molecule removed every 10, 100, and 1000 timesteps (0.05 τ, 0.5 τ, and 5 τ, respectively). The simulations are denoted X-10, X-100, and X-1000, respectively, where X denotes the system index (FOCTS, glass or PEG). For example, FOCTS-10 means evaporation of the droplet on the FOCTS surface with a deletion rate of one vapor molecule every 10 timesteps.

The second system is the adsorption of the microgel on the substrate from the bulk. We used it to simulate the deposition of the microgel through adsorption without evaporation of the solvent. The initial configuration is as follows: the single swollen microgel is placed closed to the water/substrate interface. The density of the water phase is related to the density of the fluid in the droplet. Varying the interaction between the microgel and the substrate allows us to find the ε_{MS} values describing the FOCTS, glass or PEG surface. We made a comparison of the shapes of the experimental and simulated microgels by matching the ratio of the volume of the fitted sphere cap to its ideal sphere volume for the three different substrates. All snapshots are obtained using the Open Visualization Tool (OVITO).[S14]

3. Analysis of the volume ratio

LSQR approximation of the surface

To approximate the shape of droplets as well as microgel in simulations, we define the surface points of the droplet (or microgel) and perform the ellipsoid fitting using the least-squares fitting procedure. First, we centered the droplet (or microgel) in the box such a way that the x and y coordinate of the center of mass of the droplet (or microgel) coincides with $0.5\ L_x$ and $0.5\ L_y$, respectively (Figure S3). Then, we employed an average-based approach to estimate surface points. We divided the $Z = 0$ plane into squares of equal area $\mathrm{d}X \cdot \mathrm{d}Y$ and calculated the density profiles along the z-axis (Figure S3B). We monitor the density of water (polymer) fraction and estimate the group of points on the surface within the vicinity of $Z_{\mathrm{surf}}|_{\mathrm{d}X\mathrm{d}Y}$. Based on the obtained set of surface points (Figure S3C) of the droplet (microgel) we try to fit it by the spherical surface (Figure S3D).

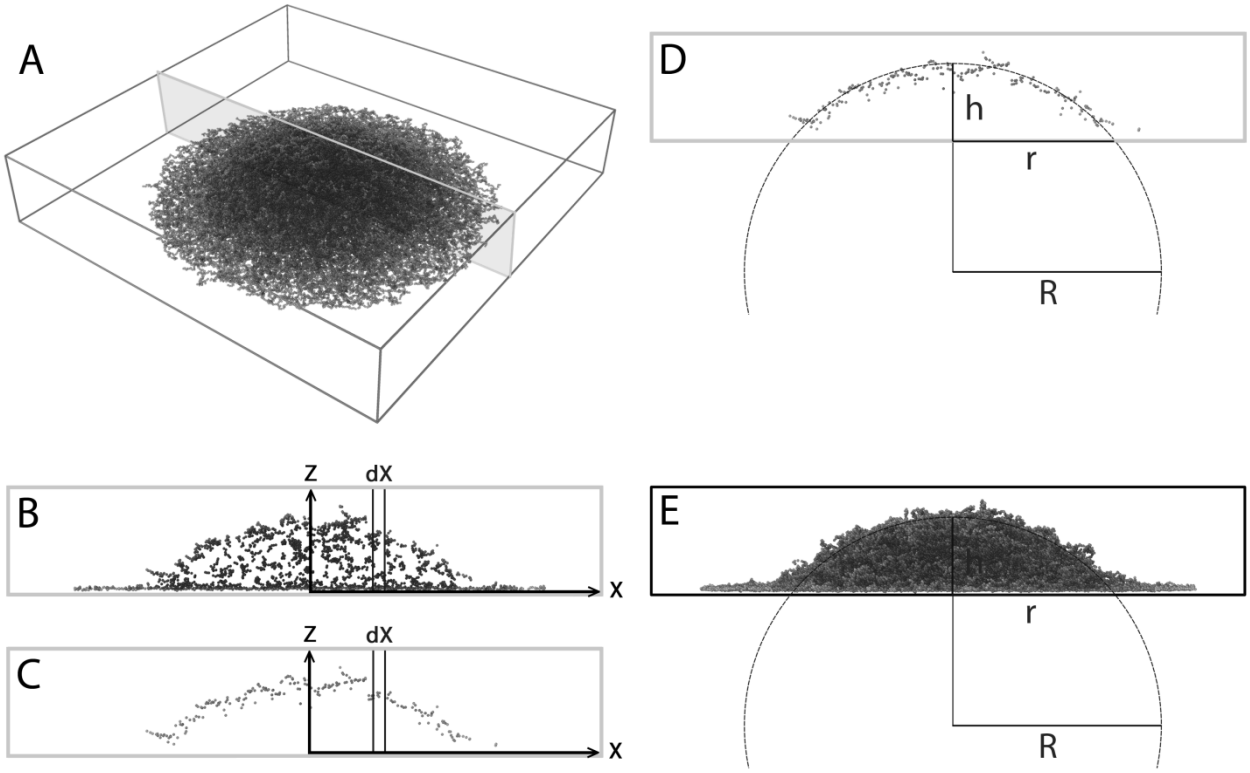

Figure S3: Surface fitting of the droplet and a microgel. A) The equilibrium structure of the microgel on the FOCTS surface obtained by the MD simulation; B) Cross-section of thickness $\mathrm{d}y = 2$ of the microgel through the center of mass $y = 0$; C) the estimated surface points of the microgel; D) the slice of the sphere found by solving the least-squares problem; E) side view of the sphere and the total microgel.

In a general case, 9 parameters describe the ellipsoid algebraically:

$$A_1x^2 + A_2y^2 + A_3z^2 + 2A_4xy + 2A_5xz + 2A_6yz + 2A_7x + 2A_8y + 2A_9z = 1 \quad (6)$$

In our case, the system is simplified to 4 parameters:

$$A_1(x^2 + y^2 + z^2) + 2A_2x + 2A_3y + 2A_4z = 1 \quad (7)$$

Now, we have a deal with the overdetermined linear equations:

$$DA = I \quad (8)$$

where A is a vector consisting of desired ellipsoid parameters, I is unity vector and D is a matrix based on the combination of surface points

$$A = \begin{bmatrix} A_1 \\ A_2 \\ A_3 \\ A_4 \end{bmatrix};\ D = \begin{bmatrix} {x_1}^2 + {y_1}^2 + {z_1}^2, & \dots \\ 2x_1 & , \dots \\ 2y_1 & , \dots \\ 2z_1 & , \dots \end{bmatrix};\ I = \begin{bmatrix} 1 \\ 1 \\ 1 \\ 1 \end{bmatrix} \quad (9)$$

Then, we attempt to solve the least-squares problem $min\|(I - A \cdot D)\|$ using the method from ref. S15. We fixed the stopping rules Dtol = 10^{-6} (an estimate of the relative error in the data defining the matrix D), Itol = 10^{-8} (an estimate of the relative error in the data defining the vector I), conlim = 10^7 and itlim = 10^4 (an upper limit on the number of iterations)

Contact angle measurements

After approximation, the contact angle

$$\theta = 90^0 + arctan\frac{h-R}{r} \quad (10)$$

can be obtained by measuring the base *r*, the height *h* and the radius *R* of the approximated sphere around the droplet (see Fig. S4).

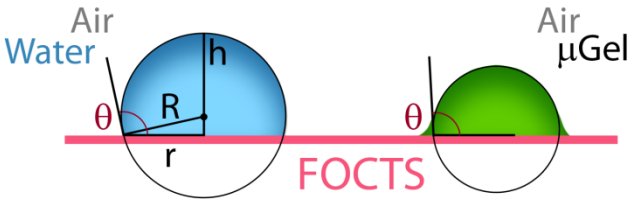

Figure S4: Geometrical measurement of the contact angle. The contact angle can be determined by measuring the diameter of the base, *r*, and the height, *h*.

The geometrical measurement is used for the volume and contact angle determination to compare the simulation and experimental results.

4. Contact Angle measurements of the solid supports

The static contact angles addressed in Fig.1 of the main paper are obtained by investigation of 3 × 5 µL drops of pure water on each of the surfaces. Images of these drops are analyzed using the Drop Snake program.[S16]

5. Volume fraction estimation

To estimate the volume fraction ($\varphi_{\mu G}$) of the µG dispersions, we performed wide-field microscopy with the stock solution counting the µGs in the defined field of view several times to obtain sufficient statistics. Apart from the xy-field of view, we estimated that µGs within a *z*-range of 10 µm are sufficiently close to the microscope focus to be identified as single µGs. The µG volume was calculated using the respective DLS data[S9] at room temperature, which gives a diameter of 1.6 ± 0.2 µm.
The number of µGs in the observed volume was multiplied with the average volume per µG and devided by the observation volume to obtain $\varphi_{\mu G}$. The calculated volume fractions for the respective deposition method are $2.0 \pm 0.6 \times 10^{-5}$ for adsorption, $7.9 \pm 2.2 \times 10^{-6}$ for drop-casting, and $4.0 \pm 1.1 \times 10^{-5}$ for spin-coating.

6. Determination of the contact area from SRFM point clouds

To estimate the radius of a contact area of the microgel we used the following method. We build the *xy*-cross-section of the cloud points of each microgel for 80 nm thick layer next to the surface. We analyzed the *xy*-coordinates of the points constructing the symmetric 2D gyration tensor **S**:

$$\mathbf{S} = \frac{1}{N}\sum_{i=1}^{N} \boldsymbol{s}_i \boldsymbol{s}_i^T = \overline{\boldsymbol{s}\boldsymbol{s}^T} = \begin{pmatrix} \overline{x^2} & \overline{xy} \\ \overline{yx} & y^2 \end{pmatrix} = \begin{pmatrix} \frac{1}{N}\sum_{i=1}^{N}(x_i - \bar{x})^2 & \frac{1}{N}\sum_{i=1}^{N}(x_i - \bar{x})(y_i - \bar{y}) \\ \frac{1}{N}\sum_{i=1}^{N}(x_i - \bar{x})(y_i - \bar{y}) & \frac{1}{N}\sum_{i=1}^{N}(y_i - \bar{y})^2 \end{pmatrix}$$

where $\boldsymbol{s}_i = \begin{bmatrix} x_i - \bar{x} \\ y_i - \bar{y} \end{bmatrix}$ is the position vector of each point in the cross-section which is considered with respect to the center of mass of the layer $\sum_{i=1}^{N} \boldsymbol{s}_i = 0$, and the overbars denote an average over all points *N* in the layer of thickness 80 nm. The diagonalization of the tensor allows us to obtain two real non-negative eigenvalues, $\lambda_x = \overline{X^2}, \lambda_y = \overline{Y^2}$. The corresponding eigenvectors, $\bar{T}_1, \bar{T}_2$ are the mutually orthogonal principal axes. In the case of a circle, $\lambda_x = \lambda_y$. These eigenvalues correspond to the variances of the coordinates along the principal axes.

We analyzed the first invariant of S,

$\mathrm{tr}\,(\mathbf{S}) \equiv I_1 = \lambda_x + \lambda_y = R_g^2$,

which gives the squared radius of gyration of the cloud (see Fig. 4 of the main paper).

7. Super-resolved localizations of labels of single microgels on PEG

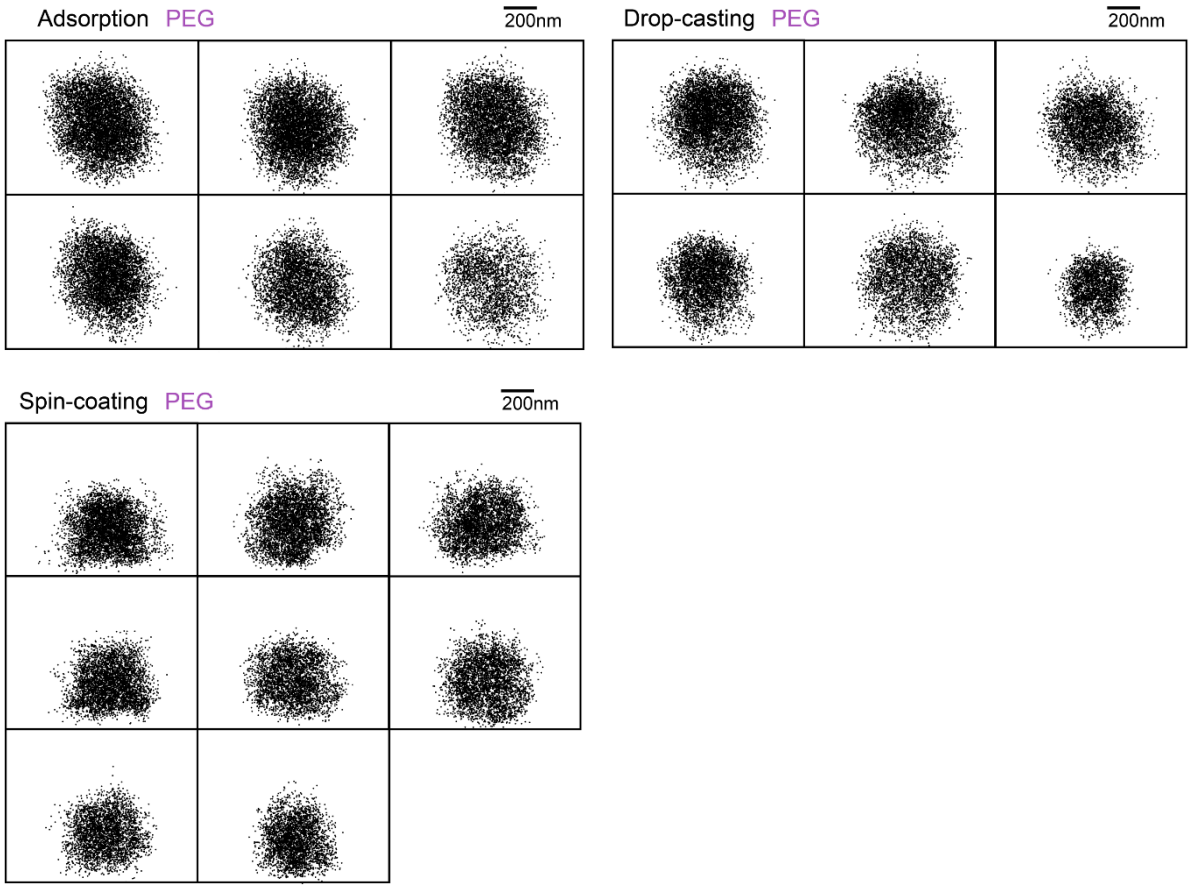

Figure S5: Cross-section profiles the SRFM point clouds of pNIPMAM µGs deposited on PEG via adsorption, drop-casting and spin-coating, respectively. The width of cross-section is 100 nm.

8. Super-resolved localizations of labels of single microgels on glass

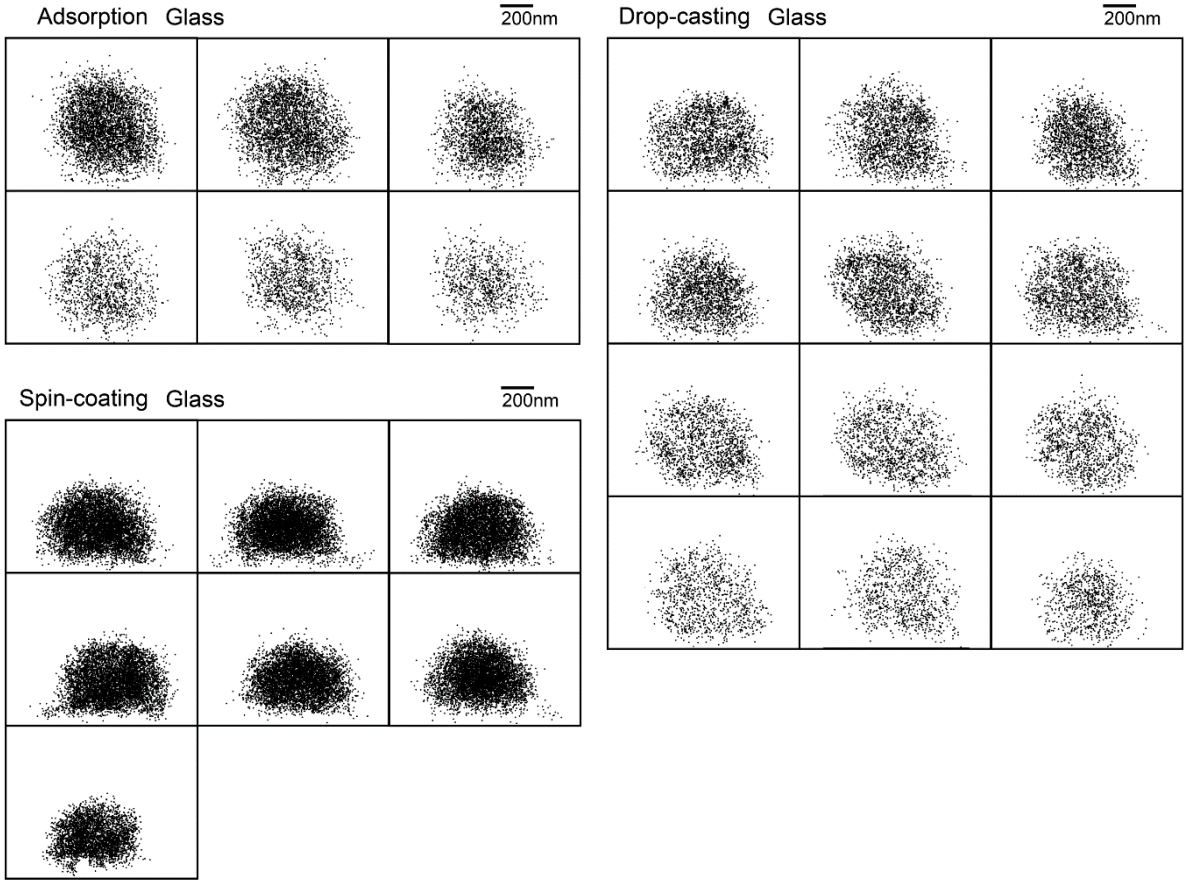

Figure S6: Cross-section profiles the SRFM point clouds of pNIPMAM μGs deposited on glass via adsorption, drop-casting and spin-coating, respectively. The width of cross-section is 100 nm.

9. Super-resolved localizations of labels of single microgels on FOTCS

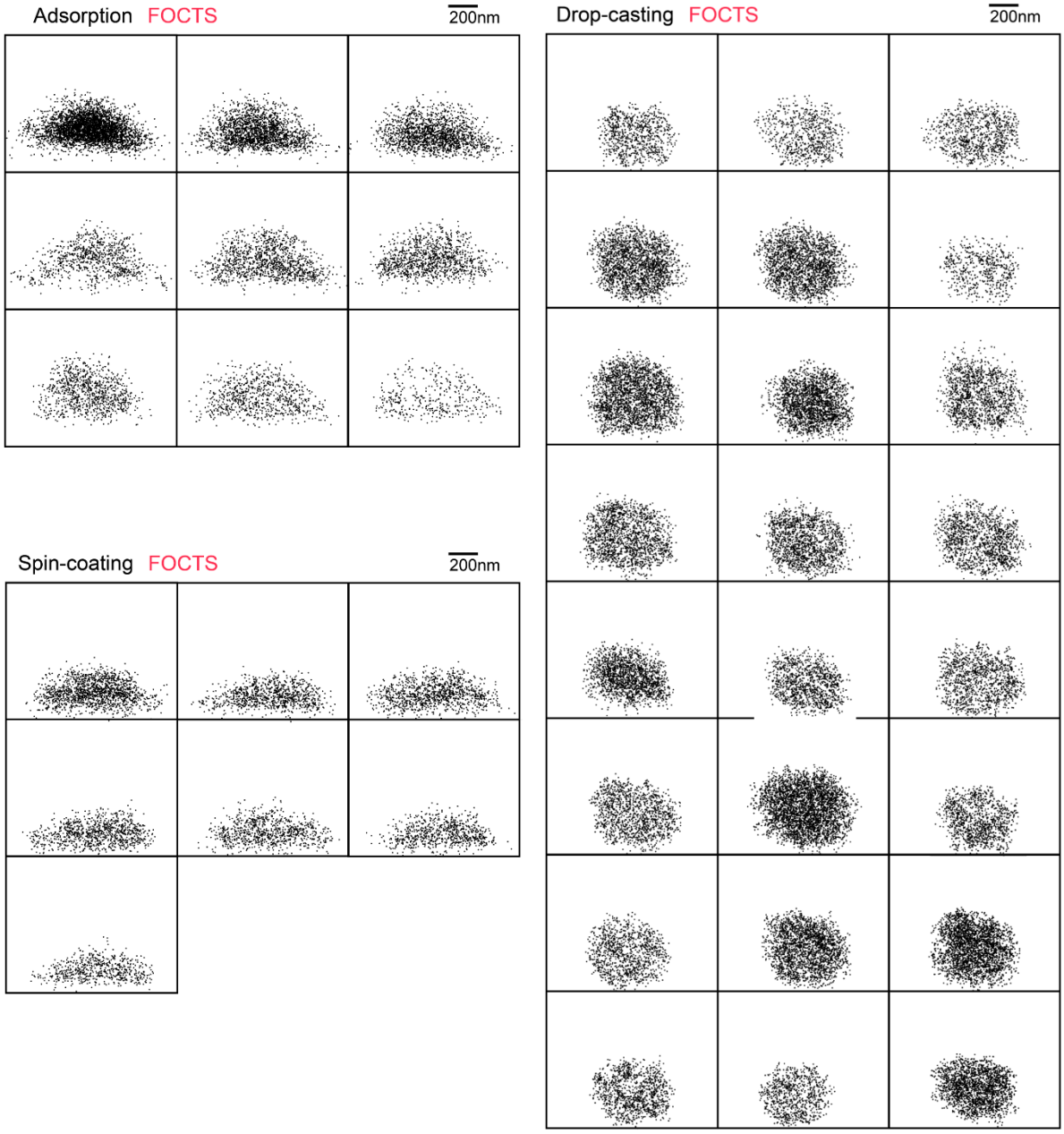

Figure S7: Cross-section profiles the SRFM point clouds of pNIPMAM μGs deposited on FOTCS via adsorption, drop-casting and spin-coating, respectively. The width of cross-section is 100 nm.

10. Supporting Literature

[S1] S. Plimton, Fast Parallel Algorithms for Short-Range Molecular Dynamics, *J. Comput. Phys.*, 1995, **117**, 1–19.

[S2] J. A. Van Meel, A. J. Page, R. P. Sear, D. Frenkel, Two-step vapor-crystal nucleation close below triple point, *J. Chem. Phys.*, 2008, **129**, 204505.

[S3] J. Vrabec, G. K. Kedia, G. Fuchs, H. Hasse, Comprehensive study of the vapour-liquid coexistence of the truncated and shifted Lennard-Jones fluid including planar and spherical interface properties, *Mol. Phys.*, 2006, **104**, 1509–1527.

[S4] W. Chen, J. Koplik, I. Kretzschmar, Molecular dynamics simulations of the evaporation of particle-laden droplets, *Phys. Rev. E*, 2013, **87**, 052404.

[S5] M. Svoboda, A. Malijevský, M. Lísal, Wetting properties of molecularly rough surfaces, *J. Chem. Phys.*, 2015, **143**, 104701.

[S6] J. Zhang, F. Leroy, F. Müller-Plathe, Evaporation of nanodroplets on heated substrates: A molecular dynamics simulation study, *Langmuir*, 2013, **29**, 9770–9782.

[S7] A. E. A. S. Evangelopoulos, A. N. Rissanou, E. Glynos, I. A. Bitsanis, S. H. Anastasiadis, V. Koutsos, Wetting Behavior of Polymer Droplets: Effects of Droplet Size and Chain Length, *Macromolecules* 2018, **51**, 2805–2816.

[S8] S. N. Sun, H. M. Urbassek, Impact desolvation of polymers embedded in nanodroplets, *J. Phys. Chem. B.*, 2011 **115**, 13280–13286.

[S9] L. Hoppe Alvarez, S. Eisold, R. A. Gumerov, M. Strauch, A. A. Rudov, P. Lenssen, D. Merhof, I. I. Potemkin, U. Simon, D. Wöll, Deformation of Microgels at Solid-Liquid Interfaces Visualized in Three-Dimension, *Nano Lett.*, 2019, **19**, 8862–8867.

[S10] N. V. Bushuev, R. A. Gumerov, S. Bochenek, A. Pich, W. Richtering, I. I. Potemkin, Compression and Ordering of Microgels in Monolayers Formed at Liquid-Liquid Interfaces: Computer Simulation Studies, *ACS Appl. Mater. Interfaces*, 2020, **12**, 19903–19915.

[S11] X. Yong, L. T. Zhang, Nanoscale wetting on groove-patterned surfaces, *Langmuir*, 2009, **25**, 5045–5053.

[S12] B. A. Noble, B. Raeymaekers, Polymer Spreading on Unidirectionally Nanotextured Substrates Using Molecular Dynamics, *Langmuir*, 2019, **35**, 8784–8789.

[S13] S. Becker, H. M. Urbassek, M. Horsch, H. Hasse, Contact angle of sessile drops in Lennard-Jones systems, *Langmuir*, 2014, **30**, 13606–13614.

[S14] A. Stukowski, Visualization and analysis of atomistic simulation data with OVITO-the Open Visualization Tool, *Model. Simul. Mater. Sci. Eng.*, 2009, **18**, 015012.

[S15] C. C. Paige, M. A. Saunders, LSQR: An Algorithm for Sparse Linear Equations and Sparse Least Squares, *ACM Trans. Math. Softw.*, 1982, **8**, 43–71.

[S16] A.F. Stalder, G. Kulik, D. Sage, L. Barbieri, P. Hoffmann, A snake-based approach to accurate determination of both contact points and contact angles, *Colloids Surf. A Physicochem. Eng. Asp.*, 2006, **286**, 92-103.